Supplementary Materials for

Systemic cancer therapy with engineered adenovirus that evades innate immunity

Svetlana Atasheva, Corey C. Emerson, Jia Yao, Cedrick Young, Phoebe L. Stewart*, and Dmitry M. Shayakhmetov*

*Correspondence to: pls47@case.edu or dmitryshay@emory.edu

This PDF file includes:

Fig. S14. Intravenous administration replication competent Ad5/35-3M virus does not trigger systemic toxicity.

Fig. S15. Human sera with high HAdv-C5-specific neutralizing antibody titers neutralize Ad5-WT and capsid-modified adenoviruses.

Other Supplementary Materials for this manuscript include the following:

(available at

Table S1. (Microsoft Excel format). Statistical summary report.

Table S2. Mouse strains used in the study.

Table S3. List of antibodies used in the study.

Table S4. Sequences of the qPCR primers.

Date file S1. (Microsoft Excel format). Primary data for Main Figures of the paper.

Data file S2. (Microsoft Excel format). Primary data for figures shown in Supplementary Materials.

Materials and Methods:

Generation of model coordinates for the Ad5-3M hexon capsid protein. In order to generate model coordinates for the Ad5-3M hexon, we started with the cryo-EM derived coordinates of the HAdv-C5 hexon (PDB: 6B1T), which fit well within the Ad5-3M density. Rigid body docking of coordinates into segmented regions of cryo-EM density was performed with UCSF Chimera (*56*). The residue numbers were adjusted in accordance with the shortened hexon HVR1 (Fig. S2) and sequence mutations were made as needed. The energy minimization component of Molecular Dynamics Flexible Fitting (MDFF) (*57*) was used to guide the coordinates of a hexon trimer into better agreement with the Ad5-3M cryo-EM density for a peripentonal hexon trimer (gscale = 0.3). A 1 ns minimization was performed and the total potential energy stabilized after ~50 ps. Next the hexon loops missing in the cryo-EM derived coordinates and present in the x-ray derived coordinates (PDB: 6CGV) were added to the Ad5-3M hexon model. All of these loops fit within the Ad5-3M cryo-EM density, although it was necessary to filter the density to 5-Å resolution with EMAN2 (*50*) to visualize the region near HVR7 (aa 413-420 in Ad5-3M). Next the sequence of the modified HVR1 was submitted to FREAD (*34*) to generate loop models. The top scoring models were visualized within the 5-Å resolution Ad5-3M hexon density and the best fitting model was selected (Figs. 2D and 2E). Another round of MDFF energy minimization (1 ns, gscale = 0.3) was performed. Again the total potential energy stabilized after ~50 ps.

Generation of model coordinates for the Ad5-3M penton base capsid protein. A similar procedure was used to generate model coordinates for the Ad5-3M penton base starting with the cryo-EM derived coordinates of the HAdv-C5 penton base (PDB: 6B1T). The residue numbers

were adjusted in accordance with the modified integrin interacting loop (Fig. S6). After rigid body docking of a pentameric version of penton base, MDFF energy minimization (1 ns, gscale = 0.3) was performed. The total potential energy stabilized after ~50 ps. Filtering the Ad5-3M cryo-EM density to 15-Å resolution with EMAN2 (*50*) revealed weak density in a protrusion extending ~28 Å above residues L296 and P381 on either end of the integrin interacting loop (Fig. 2G). This weak density accommodates ~6 extended amino acids at either end of the loop. For the five protrusions on one penton base we built five different extended models for aa 297-302 and aa 374-380 such that they spanned the observed protrusions. To fill in the missing residues of the integrin interacting loop the sequence of the middle 63 amino acids in the loop (aa 310-372) were submitted to I-TASSER (*58*). The five top scoring models were selected. These were all based on the crystal structure of the heterotrimeric integrin-binding region of laminin-111 (PDB: 5MC9). A different model was inserted at each penton base subunit and extended models were generated for the glycine-rich regions (aa303-309 and aa373-374). Some modification of the backbone torsion angles in the coil regions of the I-TASSER models was required to make the ends meet using UCSF Chimera (*56*). The energy minimization component of MDFF (*57*) (5 ps) was used to minimize the model structure with a gscale=0, since there is no cryo-EM density for the majority of the integrin interacting loop.

Molecular dynamics simulation, root mean square fluctuation (RMSF), and solvent accessibility of integrin interacting loops of Ad5-3M penton base. Following energy minimization of the Ad5-3M penton base model, a 10 ns implicit solvent molecular dynamics (MD) simulation was run with MDFF (gscale = 0) (fig. S4). During the MD simulation, the coordinates of penton base atoms in well-defined cryo-EM density were held fixed. Only the

coordinates in the integrin interacting loops plus a few adjacent residues (aa 290 to 390) were allowed to move. The CHARMM force field with default parameters was used for the simulation as described previously (*33*). The total energy of the system stabilized after ~5 ns as evaluated by NAMD (*59*).

Root mean square fluctuation (RMSF) calculations were performed to estimate the flexibility of the integrin interacting loops of penton base. One RMSF value per Cα atom was calculated with VMD (*60*) for the time range of 5 ns to 10 ns during the simulation. Microsoft Excel was used to group the values for the 6aa linker regions (aa 297-302 and aa375-380), the middle 72 aa of the integrin interacting loop including the glycine-rich linkers (aa 303-374), and the integrin interacting residues SIKVAV (aa 341-346) and average among all five penton base subunits. We found RMSF values for these regions of 4.7 Å, 9.6 Å, and 10.5 Å respectively. These results indicate that the integrin-interacting SIKVAV residues in the middle of the loop display a high degree of fluctuation, which may be functionally advantageous for forming interactions with cell surface integrins.

Coordinates were saved from the 5 ns, 7.5 ns, and 10 ns time points of the MD trajectory of the penton base with modeled integrin interacting loops. The coordinates were read into ChimeraX (*61*) and the measure command was used to determine solvent accessibility with a probe radius of 1.4 Å. Values were calculated for the solvent-accessible surface area of each SIKVAV region on each penton base subunit at each of the three time points. We found that the solvent-accessible surface area of the SIKVAV residues ranges from 864 to 978 $Å^2$ with an average of 876 $Å^2$. We conclude that the engineered integrin-interacting loop of Ad5-3M likely has significant solvent accessibility for the critical integrin-interacting residues.

Cells. Non-small cell lung cancer cell lines (NSCLC) A549, CRL-5872, CRL-5939, CRL-5909, CRL-5800, CRL-5908, CRL-5887, CRL-5876, and HEK293 cells were purchased from ATCC and maintained according to ATCC recommendations. A549-luc-C8 was purchased from Caliper and maintained in Dulbecco's Modified Eagle Medium (Gibco) supplemented with 10% fetal bovine serum (Gibco).

Viruses. Recombinant viruses were cloned using a recombineering platform from Dr. Anja Ehrhardt's lab (*62*) with several modifications. Briefly, all viruses were assembled in two steps. In the first step a PCR product encoding the kanamycin resistance gene (kan^R) flanked with SwaI restriction sites (absent in HAdv-C5 genome) and ~50 nt of homologous sequence of the region of intended insertion was electroporated in *E. coli* strain SW102 containing a bacterial artificial chromosome (chl^R) with HAdv-C5 genome. For the second step, DNA from the kan^R/chl^R colonies was cut with SwaI and electroporated simultaneously with a double-strand DNA fragment (gBlock, IDT) containing a desired sequence flanked with ~200 nt of homologous sequences into BJ5183 *E.coli* strain. The chl^R colonies were screened for correct clones. The clones were sequenced to confirm introduced mutations. To produce viruses, the isolated DNA of the sequenced clones was cut with PacI and transfected into HEK293 cells. After propagation viruses were isolated from crude cell lysate treated with Benzonase nuclease (SigmaAldrich) following with double banding on a cesium chloride gradient described elsewhere (*63*). The cesium chloride was replaced with a storage buffer (10mM Tris, 1mM $MgCl_2$, 150 mM NaCl, 5% sucrose) using Zeba spin desalting columns, 40K (ThermoFisher). Viruses were aliquoted and stored at -80C^0. The virus titers were calculated by measuring

optical density of the solution of SDS-disrupted virions following ratio 1 OD_{260} = $1.1x10^{12}$ viral particles (vp)/ml.

Virus transduction in vitro. Different cells lines were seeded on 96 well plates and infected with Ad5-WT or Ad5-3M viruses with multiplicity of infection (MOI) of 10, 100, and 1,000 of vp/cell. Propidium iodide (PI) was added to the media (4 μg/ml) to track cells that undergo necrotic death. Plates were loaded into the IncuCyte Zoom live-cell analysis system (Essen Bioscience) and imaged every 2 h for virus replication-dependent GFP expression and necrosis-induced PI intercalation into the DNA for 4 days. The images were analyzed and extracted using IncuCyte Zoom 2016B software (Essen Bioscience). Viruses incubated with mouse or human sera, as described below, were diluted 2,000 fold and added to HEK293 cells in 24 well plates. Plates were loaded into the IncuCyte Zoom live-cell analysis system (Essen Bioscience) and GFP-positive cells were counted at 20 h post infection.

ELISA assay. Serum IgM have an extreme propensity to nonspecifically adhere to coated surfaces of the 96 well plates. To decrease IgM, and subsequent C4 and C3 nonspecific binding, all reactions were performed in solution in a tube, then the reaction was stopped by diluting ten-fold and opsonized virions with attached proteins were captured with the Coxsackie and adenovirus receptor (CAR) protein coated plates. In more detail, the 96 well plates were coated with recombinant CAR-His (Sino Biological, #10799-H08H) 2 μg/ml in PBS for 2 h at $37C^0$. After coating the wells were blocked with 10% goat serum in PBS for 4 h at $37C^0$. All reactions were performed with freshly harvested, never frozen EDTA-preserved plasma or serum that was pooled from several mice for each experiment. Each test was done in at least 3 separate

experiments. The total volume of reaction was 50 µl with 90% serum or plasma and $2x10^9$ viral particles. The reaction was held for 30 min at $37C^0$, after 30 min incubation it was diluted ten-fold with PBS/10 mM EDTA/0.05% Tween20 and the virus with attached protein complexes was captured overnight on plates coated with CAR, with constant agitation at $4C^0$. Next day the inoculum was washed away and IgM, C3, or C4 were detected using specific antibodies with conjugated horseradish peroxidase (HRP). The colorimetric reaction was performed with 1-step TMB substrate (ThermoFisher) and OD450 was measured on Synergy HTX plate reader (BioTek) using Gen5 software (version 2.06.10). Complement deposition in human serum was measured the same way using purchased frozen human serum from Innovative Research and using human C3- specific antibody.

Immunostaining of tissue sections and cells. Freshly isolated tissues were immediately frozen in Tissue-Tek optimal cutting temperature (OCT) compound (Sakura) and kept at $-80C^0$ before cutting slides. The tissue slides with thickness of 8-12 micron were cut using a CM1860 UV microtome (Leica). The tissue slides were dried overnight at room temperature and fixed with acetone at $-20C^0$. After hydration, the slides were incubated with different antibodies at 1:100 dilution in 5% goat serum in Tris- buffered saline solution for 16 h at $4C^0$. All antibodies used in the study are listed in **Table S3**. After primary antibody staining the slides were washed and incubated with secondary antibody if necessary. A nonspecific tissue autofluorescence was quenched by incubation of the samples in 0.1% Sudan black B (Sigma-Aldrich), after extensive washing, the slides were mounted with Prolong Gold antifade reagent with or without DAPI (Invitrogen). The pictures were taken on Axio Imager Z2 microscope (Zeiss) using either Plan-Apochromat 20x/0.8M27, EC Plan-Neofluor 40x/0.75 M27, or Plan-Apochromat 100x/1.4 Oli

DIC M27 lenses (Zeiss). The pictures for calculating Kupffer cell-associated virus were not further adjusted in any way. The pictures for publication were taken using Apotome.2 optical sectioning system (Zeiss) and exported using Zen 2012 Blue edition software (Zeiss).

Virus infection of monocyte derived human macrophages. Three different batches of cryopreserved positively-selected CD14+ human peripheral blood monocytes were purchased from Lonza and maintained in RPMI 1640 media supplemented with 10% heat inactivated fetal bovine serum. Monocytes were differentiated in the presence of 40 ng/ml hGM-CSF (R&D systems) and 20U/ml of DNAse (Sigma-Aldrich) for seven days (*64*). $2x10^5$ of differentiated macrophages were plated on 12-well-plates overnight and infected with viruses preincubated with raw naïve human serum. To select a naïve human serum, 40 different human serums were purchased from Innovative Research and tested for neutralization activity against Ad5-WT. Eight serums did not demonstrate virus neutralization and one serum out of eight did not deposit antibody and complement C3 on Ad5-WT, we defined this serum as a naïve human serum. $2x10^9$ vp in 5 μl volume of Ad5-WT or Ad5-3M were incubated with 90% raw naïve human serum for 30 minutes at 37^0C and the mix was added to plated differentiated macrophages. After two hours the wells were rinsed and incubated in the presence of 20 ng/ml hGM-CSF, in 72 h the supernatants were harvested and the concentration of cytokines and chemokines was measured.

Analysis of anti-tumor activity of viruses in mouse tumor models. For subcutaneous tumor model 8 weeks old female NSG mice (The Jackson Laboratory) were injected sc with $5x10^6$ A549-Luc-C8 cells. For establishing the patient-derived xenograft (PDX) tumor models the

PDX-bearing mice were purchased from The Jackson Laboratory (PDX models used in the study TM00302, TM00784, TM00219, TM00233). Upon reaching a volume of ~ 1,500 mm^3, the PDX tumors were excised, cleaned of connective and/or necrotic tissue, sliced in small pieces and subcutaneously implanted in naïve NSG mice (*65*). To test virus transduction efficiency, small pieces of PDX tissues were placed in standard growing media and incubated with Ad5-3M virus in 12 well plates. Virus-dependent GFP expression was monitored and pictures were taken with either widefield microscope or scanned on IncuCyte Zoom live-cell analysis system (Essen Bioscience) 3-5 days post infection. The tumor growth of PDX- or A549-Luc-C8-derived tumors was closely monitored and when subcutaneous tumors reached mean volumes 37.79 ± 23.27 mm^3 (PDX-TM00302), 443.2 ± 135.7 mm^3 (PDX-TM00784), 298.1± 146.3 mm^3 (A549), mice were randomized and divided in cohorts. The Ad5-3M-treated cohorts were injected intravenously via tail vein with 3 doses of the Ad5-3M virus, each dose containing $2x10^{10}$ vp and separated by 48 h. The buffer cohort mice were injected with the same regiment, but with a buffer solution. In Ad5-WT-treated cohorts mice were injected with two doses of virus, each dose containing $2x10^{10}$ vp and all mice succumbed to virus-induced hepatotoxicity before the third dose injection. The tumors were measured with electronic calipers and tumor volume was calculated by the formula ((tumor width (mm))^2*tumor length(mm))/2. The mice were sacrificed when tumor volume reached 2,000 mm^3 or tumor-burden score >17 (Emory University institutional IACUC guidelines).

For the orthotopic disseminated cancer model 8-12 weeks old female athymic NCr nude mice (Taconic Biosciences) were injected intravenously (i.v.) via tail vein with $3x10^6$ A549-Luc-C8 cells, expressing firefly luciferase gene. In 5 weeks after tumor cell implantation the tumor burden was measured by *in vivo* bioluminescent imaging (BLI). Only tumor-bearing mice

with luciferase activity measured at 2-8x10^6 ph/sec/cm^2/sr were enrolled in the experiment. Enrolled mice were randomized and divided in cohorts. The Ad5-3M cohort mice were injected with 3 doses of the virus i.v. via tail vein, each dose containing 1x10^{11} vp and administered over 48 h intervals. In the Ad5/35-3M cohort, mice received the same regimen, but each dose was equal to 5x10^{10} vp per mouse. Mice from the buffer cohort were injected similarly, but with a virus-diluent buffer only. In the Ad5-WT cohort, mice were injected with 1x10^{11} vp/mouse; however, all mice succumbed to virus-induced hepatotoxicity after the first virus dose, and the planned injection of a second virus dose was not performed. The tumor burden was measured by BLI weekly and mice were monitored for signs of endpoint criteria (measured firefly luciferase activity at least 1x10^8ph/sec/cm^2/sr and 20% body weight loss or episodes of dyspnea).

Non-invasive in vivo bioluminescence imaging (BLI) of animals. Mice were anesthetized with isoflurane and injected intraorbitally with 75 mg/kg D-Luciferin, sodium salt (GoldBio) for detection of firefly luciferase or with 5 μl of the Nano-Glo substrate (Nano-Glo luciferase assay, Promega) diluted 1:10 with PBS for detection of nano-luciferase activity. After substrate injection mice were placed in the IVIS Lumina Series III (PerkinElmer) machine and imaged using Living Image 4.4 software. Luciferase activity was measured as photons/sec/cm^2/sr.

Quantitative PCR analysis. Tissue samples for qPCR were harvested and flash frozen in liquid nitrogen. For DNA isolation tissues were disrupted using a bullet blender tissue homogenizer (Next advance) and total DNA was isolated using QIAamp DNA mini kit (Qiagen) according to the manufacturer's recommendations. Viral DNA was measured using virus-specific primers,

the sequences of all primers used in the study can be found in **Table S4** (*66*). The absolute numbers of viral genomes in the samples were calculated using a standard curve. DNA for the standard curve was isolated from a mixture of a known amount of virus with 25 mg of liver tissue from a naïve mouse. The qPCR reaction was held in a 10 μl reaction with 80 ng of total DNA using SsoAdvanced Universal SYBR Green Supermix (Bio-Rad) in CFX384 thermal cycler (Bio-Rad).

Analysis of liver enzymes in mouse sera. The liver function tests were done at the Emory University Quality Assurance & Diagnostic Laboratory using Vet Axcel Chemistry Analyzer (Alfa Wassermann).

Supplementary Figures

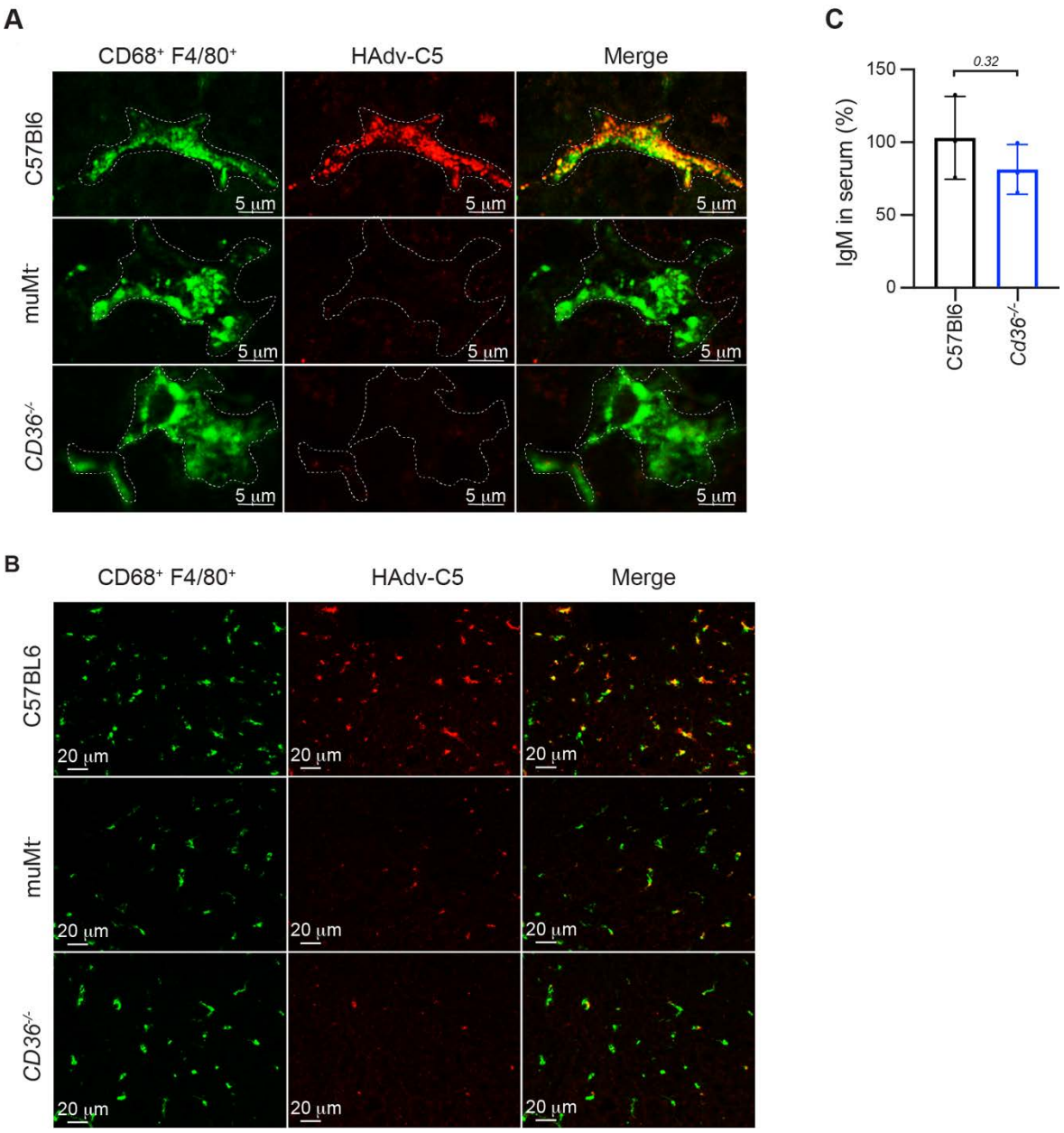

Fig. S1. Efficient HAdv-C5 virus sequestration in liver macrophages requires natural IgM antibodies and scavenger receptor CD36. (**A**) Immunofluorescent staining of sections of livers harvested from C57Bl6, µMT, and *CD36*$^{-/-}$ mice 30 minutes after intravenous injection with HAdv-C5 virus. Images of individual representative macrophage cells are shown. (**B**) is same as (A) with lower magnification to illustrate the field-of-view. Positive staining with CD68-specific and F4/80-specific antibodies, recognizing tissue macrophages, is in green. HAdv-C5-specific polyclonal antibody staining is in red. The anatomical boundary of individual macrophage cells are depicted with dotted lines. (**C**) Amounts of natural IgM in serum of wild-type C57Bl6 and *Cd36*$^{-/-}$ mice (n = 3).

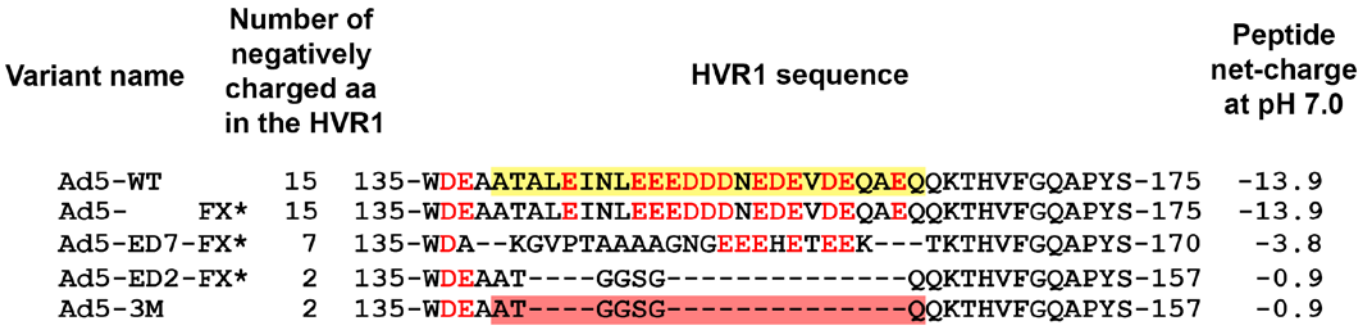

Fig. S2. Hexon HVR1 sequence comparison for viruses used in the study. The yellow highlighting denotes residues missing in the cryo-EM derived HAdv-C5 hexon coordinates (PDB: 6B1T). The red highlighting denotes residues in Ad5-3M modeled with FREAD (*34*) and displayed in red in Figs. 2D and 2E. Negatively charged residues Glu (E) and Asp (D) are shown in red.

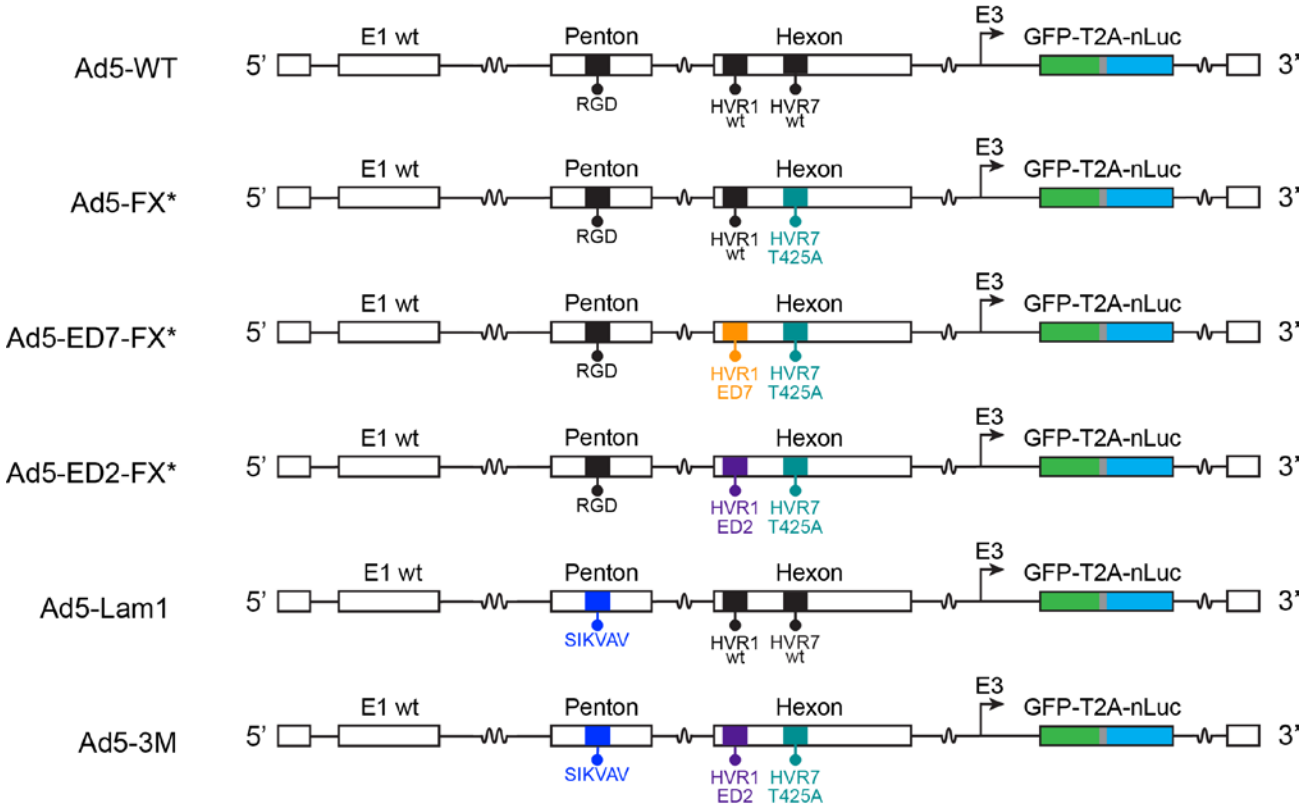

Fig. S3. Schematic diagrams of the genomic structure of viral vectors used in this study and specific mutations introduced into the hexon and penton base capsid proteins of each adenovirus variant. Ad5-WT vector has the capsid of HAdv-C5 without any modifications**.**

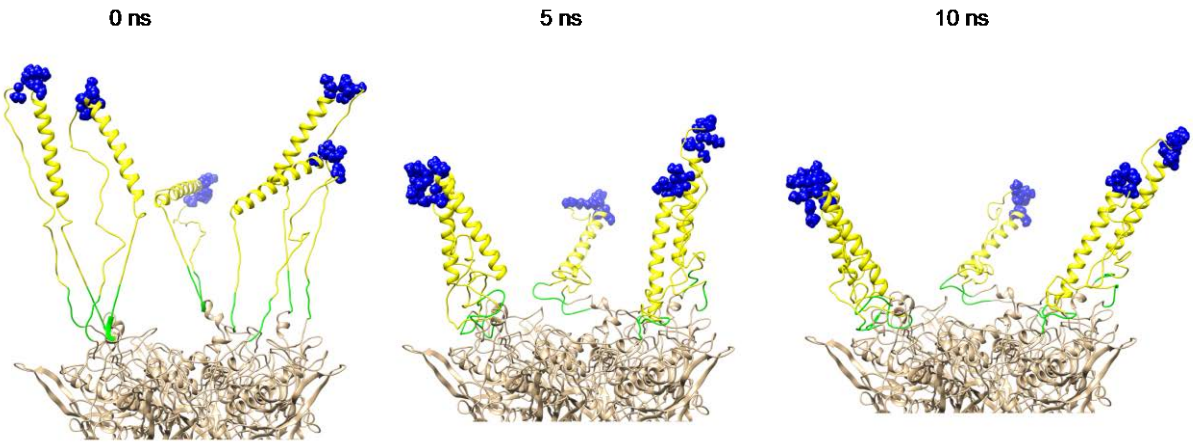

Fig. S4. Structural modeling and MD simulations of the penton base containing the Lam1 insertion. Side view of the penton base at the beginning of the simulation (0ns), at the midpoint of the simulation (5ns), and at the end of the simulation (10ns). The well-defined penton base residues are in tan, the 6aa linker regions (as defined in fig. S6) are in green, and the middle the integrin-interacting loops are in yellow with the integrin-interacting SIKVAV residues in blue space-filling representation.

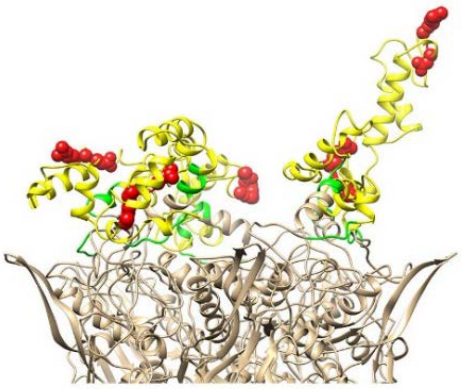

Fig. S5. Modeling of penton base loop in HAdv-C5. The modeled RGD-containing loops, (based on (*33*)), are shown on top of the HAdv-C5 penton base. The well-defined penton base residues are in tan, the 6aa linker regions (as defined in fig. S6) are in green, and the middle of the integrin-interacting loops are in yellow with the integrin-interacting RGD residues in red space-filling representation.

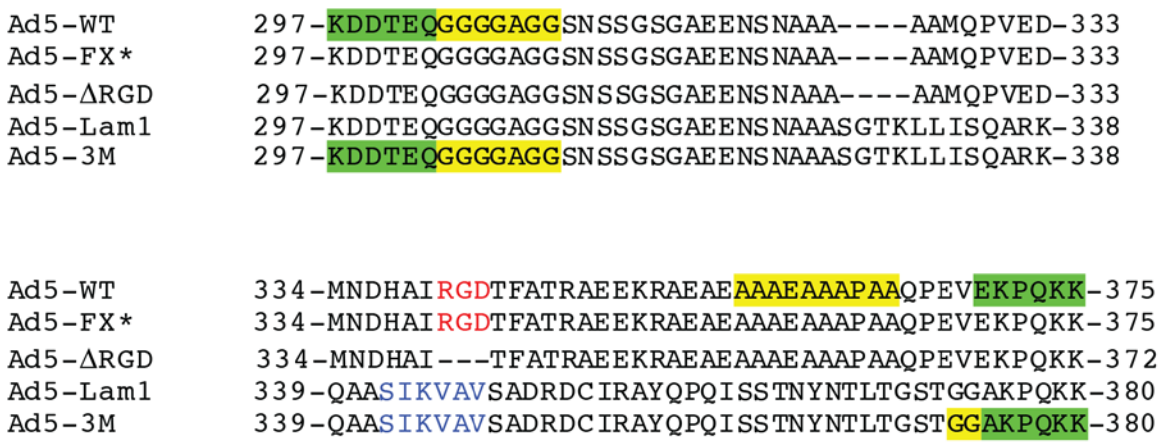

Fig. S6. Penton base loop sequence comparison for viruses used in the study. The RGD residues of Ad5-WT and Ad5-FX* are in red and the SIKVAV residues of Ad5-Lam1, and Ad5-3M are in blue. The green highlighting denotes 6aa linkers proposed to span protrusions observed on the top of penton base in the Ad5-3M cryo-EM structure (Fig. 2G). The yellow highlighting denotes glycine- and alanine-rich regions, which likely give the loops in Ad5-WT and Ad5-3M a high degree of flexibility.

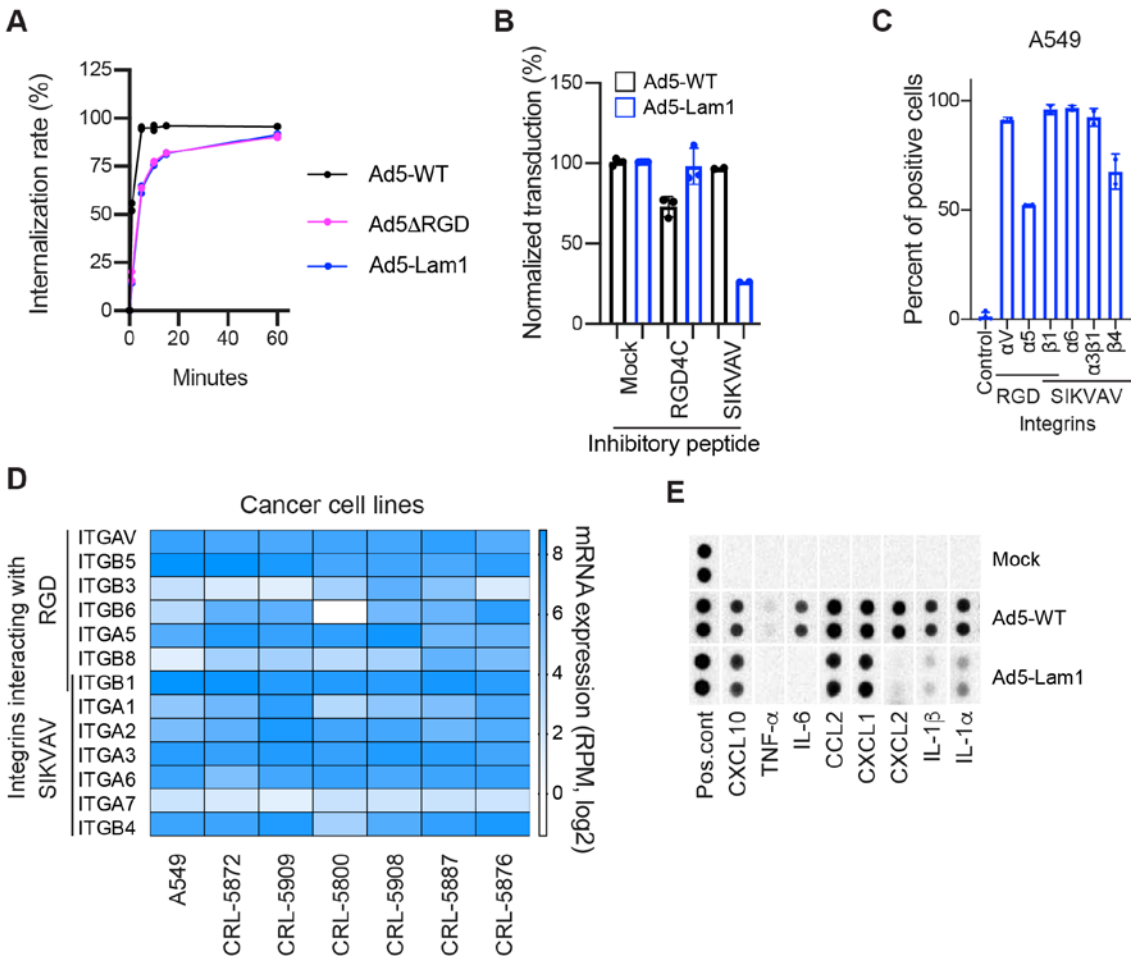

Fig. S7. HAdv-C5 de-targeting from β3- integrins reduces inflammation. (**A**) Internalization kinetics of viruses in A549 cells. Ad5-WT or viruses with modified RGD motif were incubated with A549 cells at an MOI of 1,000 vp/cell at $4C^0$. After initial attachment excess virus was washed off and cells were allowed to internalize the virus for the indicated times before the process was stopped by addition of virus-neutralizing serum. The internalization rate was measured as the portion of infected cells in samples with blocked internalization to samples with an uninterrupted internalization process. The number of infected cells was measured at 24 h post virus addition (n = 2). (**B**) Blockage of virus infection by inhibitory peptides. A549 cells were incubated with viruses in the presence of synthetic inhibitory peptides. The transduction rate was calculated at 24 h post infection (n = 2-4). (**C**) Expression of RGD or SIKVAV-interacting integrins on the surface of A549 cells. A549 cells were stained using integrin-specific antibodies (n = 2-4). (**D**) mRNA expression of RGD or SIKVAV-interacting integrins in different cancer cell lines. RPM- reads per million. (**E**) Retargeting the virus from RGD – cellular β3 integrin interaction to SIKVAV motif-dependent integrins resulted in a significant reduction in activation

of inflammatory cytokines. Protein array assay with spleen lysates isolated from mice 1 h after injection with $3x10^{10}$ vp/ mouse.

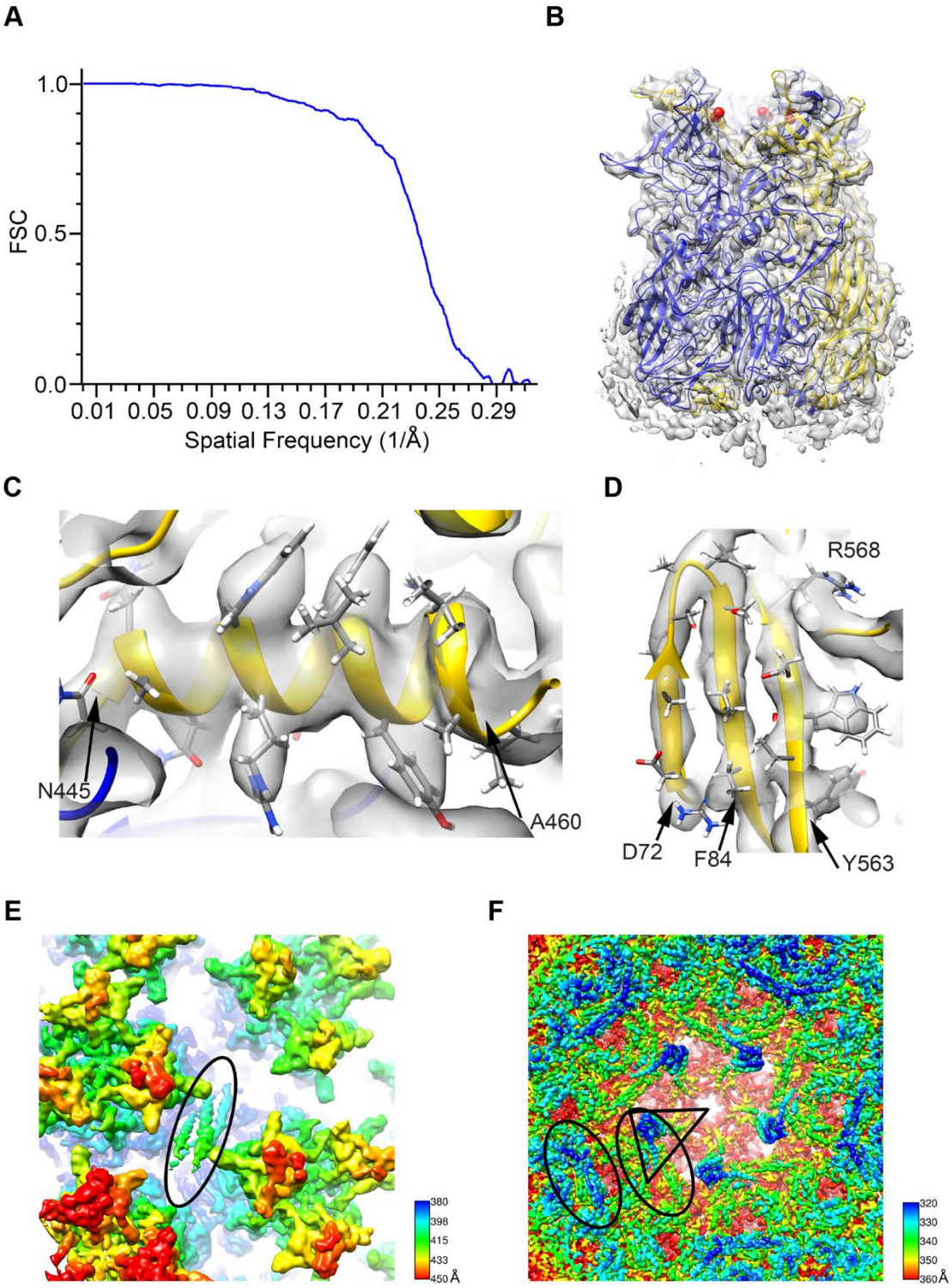

Fig. S8. Resolution assessment of Ad5-3M capsid. (**A**) Fourier Shell Correlation (FSC) plot calculated by cisTEM (*50*) indicating a resolution of 3.8-Å at the 0.143 threshold. (**B**) Side view of Ad5-3M hexon trimer model (one subunit in gold, two subunits in blue). The Ad5-3M cryo-EM density for the

peripentonal hexon is shown in transparent gray. The three Thr-425-Ala (numbered as in HAdv-C5) mutation sites in the trimer are shown in space filling representation (red). (**C**) α-helical region within the Ad5-3M hexon. The cryo-EM density (transparent gray) around aa445-460, chain A (gold) is shown together with the Ad5-3M hexon model with sidechains displayed for the α-helical residues. (**D**) β-strand region within the Ad5-3M hexon. The cryo-EM density (transparent gray) around aa72-84 and aa563-568, chain A (gold) is shown together with the Ad5-3M hexon model with sidechains displayed for the β-strand residues. Observation of large sidechain density supports the global resolution of 3.8-Å. (**E**) Density for the coiled-coil region of the minor capsid protein IX (oval), which is situated between hexons on the exterior of the capsid. (**F**) Density for protein IIIa (triangle) and protein XIII (ovals) on the inner surface of the capsid. The view is from the interior of the virion and along a 5-fold icosahedral axis. Visual comparison of the Ad5-3M and HAdv-C5 (EMD: 7034) cryo-EM density maps indicates that all of the major and minor capsid proteins of adenovirus are properly assembled within Ad5-3M.

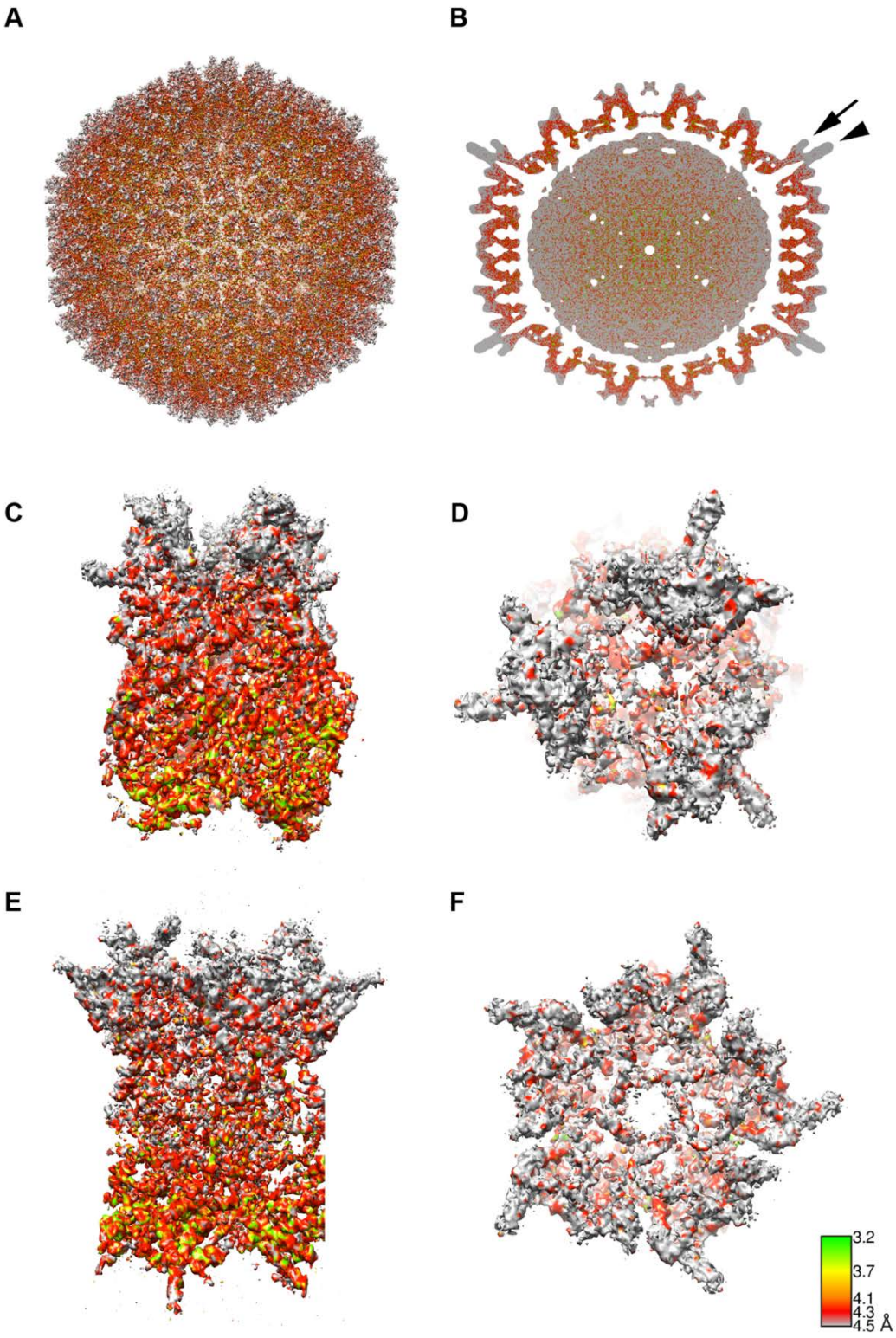

Fig. S9. Local resolution assessment of Ad5-3M. (**A**) View of the Ad5-3M capsid along a 3-fold icosahedral axis. (**B**) Gaussian smoothed view of a central plane through the virion, viewed along a 2-

fold icosahedral axis. The arrow indicates a penton base protrusion and the arrowhead points to the base of the protruding fiber. The rest of the fiber is not observed because of flexibility for the distal portion. Both the penton base protrusion and the base of the fiber are at the lowest resolution (4.5 Å). (**C** and **D**) Side and top views of the peripentonal hexon. (**E** and **F**) Side and top views of penton base. Note that the tops of the hexon and penton base are at the lowest resolution (4.5 Å). The density shown in all panels is colored based on the local resolution as calculated by MonoRes (*51*).

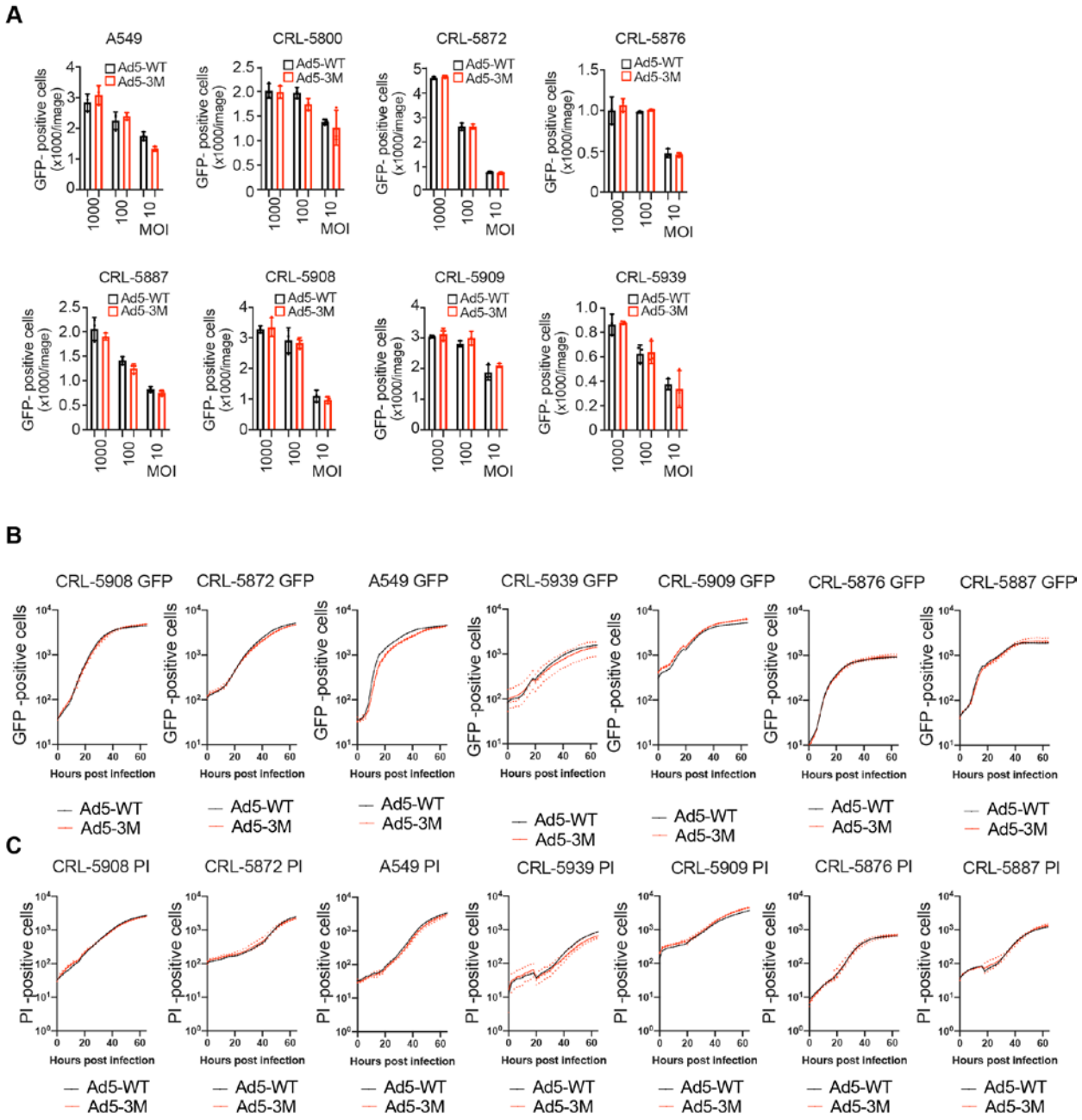

Fig. S10. Ad5-3M effectively infects a variety of non-small cell lung cancer (NSCLC) cell lines. (**A**) Comparison of transduction efficiency of Ad5-WT and Ad5-3M in a panel of NSCLC cell lines. Cancer cell lines were infected with viruses at an MOI of 10, 100, or 1,000 vp/cell and the transgene (GFP) -positive cells were counted at 24 h post infection (n = 3). (**B**) Growth curves of Ad5-WT and Ad5-3M in a panel of NSCLC cell lines. Cells were infected with Ad5-WT and Ad5-3M at an MOI of 10 vp/cell and transgene (GFP)-positive cells were counted every 2 h post infection. (**C**) Cytolytic activity of Ad5-WT and Ad5-3M. Cells were infected with viruses at an MOI of 10 vp/cell and propidium iodide (PI)-positive cells were counted with 2 hour intervals.

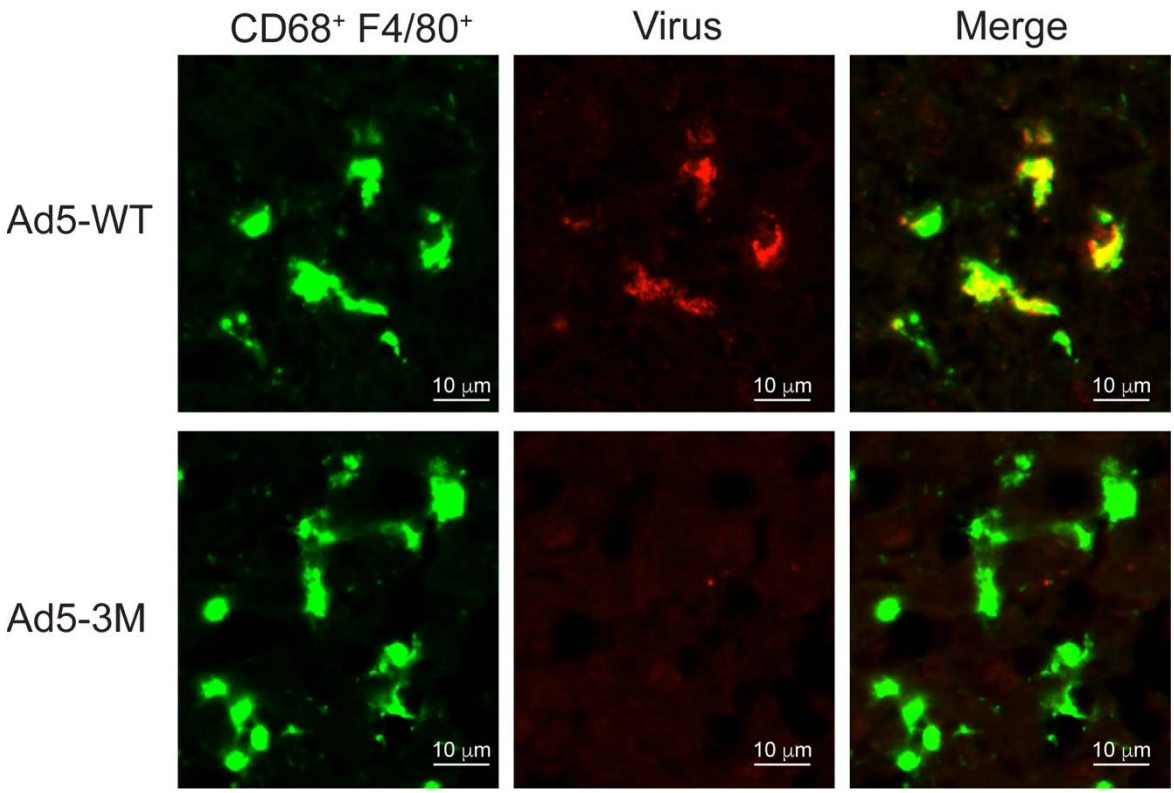

Fig. S11. Ad5-3M escapes Kupffer cell sequestration. Immunofluorescent images of the liver sections stained with anti-CD68 and anti-F4/80 antibody (green- Kupffer cells) and with poly-clonal anti-adenovirus antibody (red). Livers were harvested 30 minutes post intravenous injection of $3x10^{10}$ vp/mouse of Ad5-WT or Ad5-3M viruses.

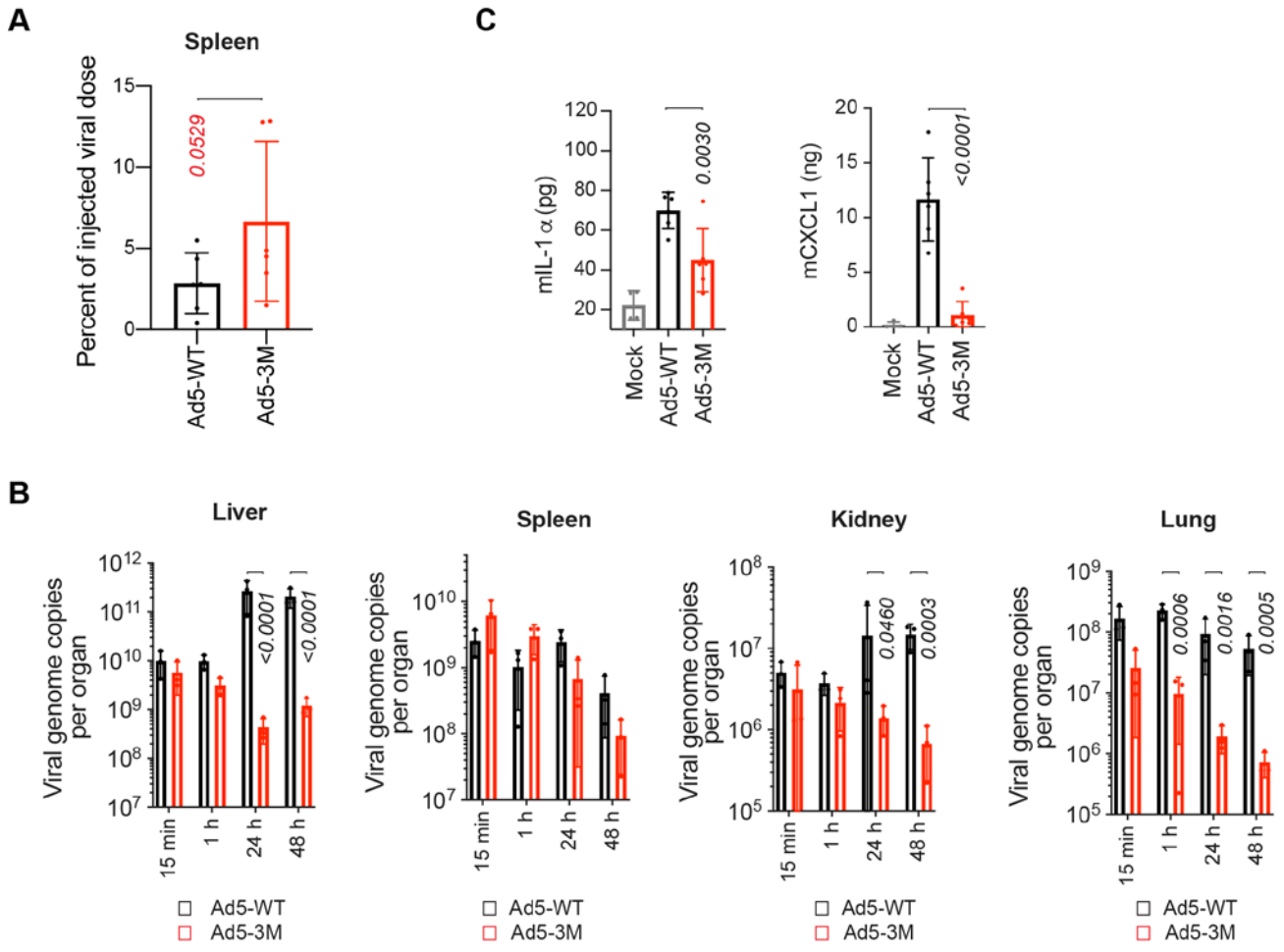

Fig. S12. Ad5-3M biodistribution after intravenous delivery. (**A**) Viral DNA detected by qPCR in the spleens. Spleens were harvested 1 hour post intravenous injection of $3x10^{10}$ vp/mouse of indicated viruses and viral genomic DNA was detected using virus-specific primers and compared to the total injected dose (n = 3-6); p = 0.0529 using one-tailed t-test analysis. (**B**) Organs were harvested at the indicated time points from mice intravenously injected with $3x10^{10}$ vp/mouse of Ad5-WT or Ad5-3M viruses and viral genomic DNA was analyzed using virus-specific primers by qPCR (n = 3). (**C**) Comparison of cytokine and chemokine concentrations in the spleens (pg or ng per 130 mg of spleen tissue) at 1 hour post intravenous virus injection (n = 4-6). Unless stated otherwise, the p-values were calculated by comparing the data from the same time point between different viruses using two-way ANOVA test on log-transformed data (B) or one-way ANOVA (C). Statistical details are in **Table S1**.

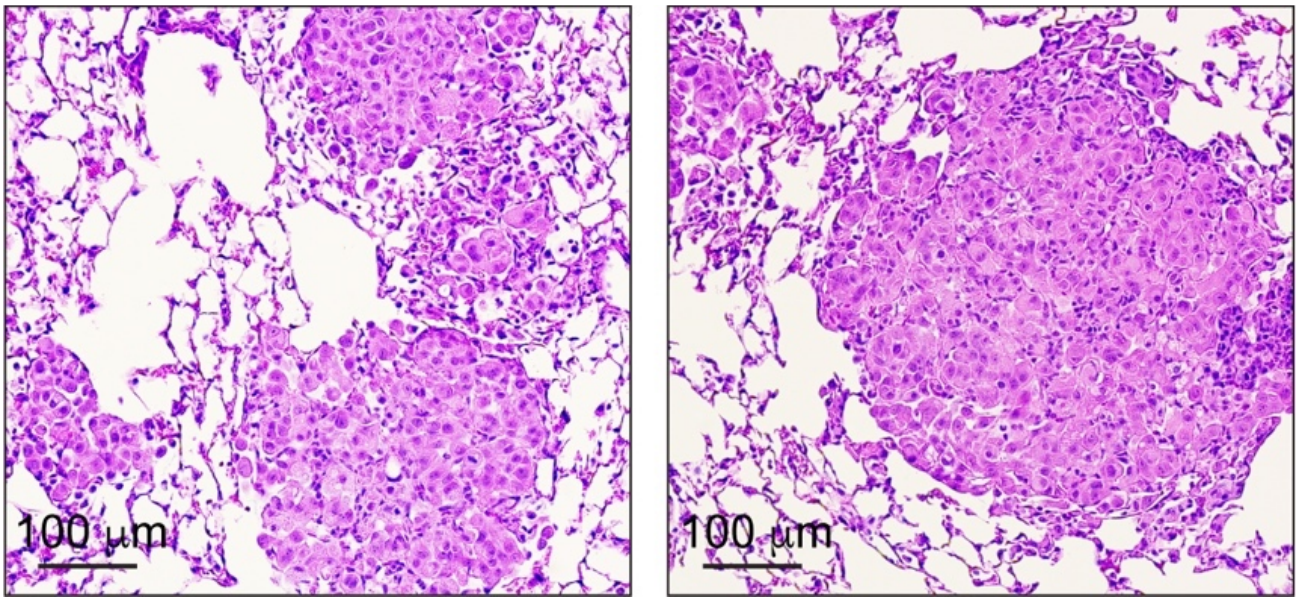

Fig. S13. A549-luc-C8 cells form tumor nodules in lungs after intravenous injection. $3x10^6$ A549-luc-C8 human lung carcinoma cells expressing firefly luciferase were intravenously injected in NCr nude mice. 5-6 weeks after implantation lungs from mice with firefly luciferase activity measured by *in vivo* BLI at $2 – 8 \times 10^6$ ph/sec/cm^2/sr were harvested and preserved in formalin. Lung sections were stained with H&E to visualize the tumor nodules and normal lung tissue.

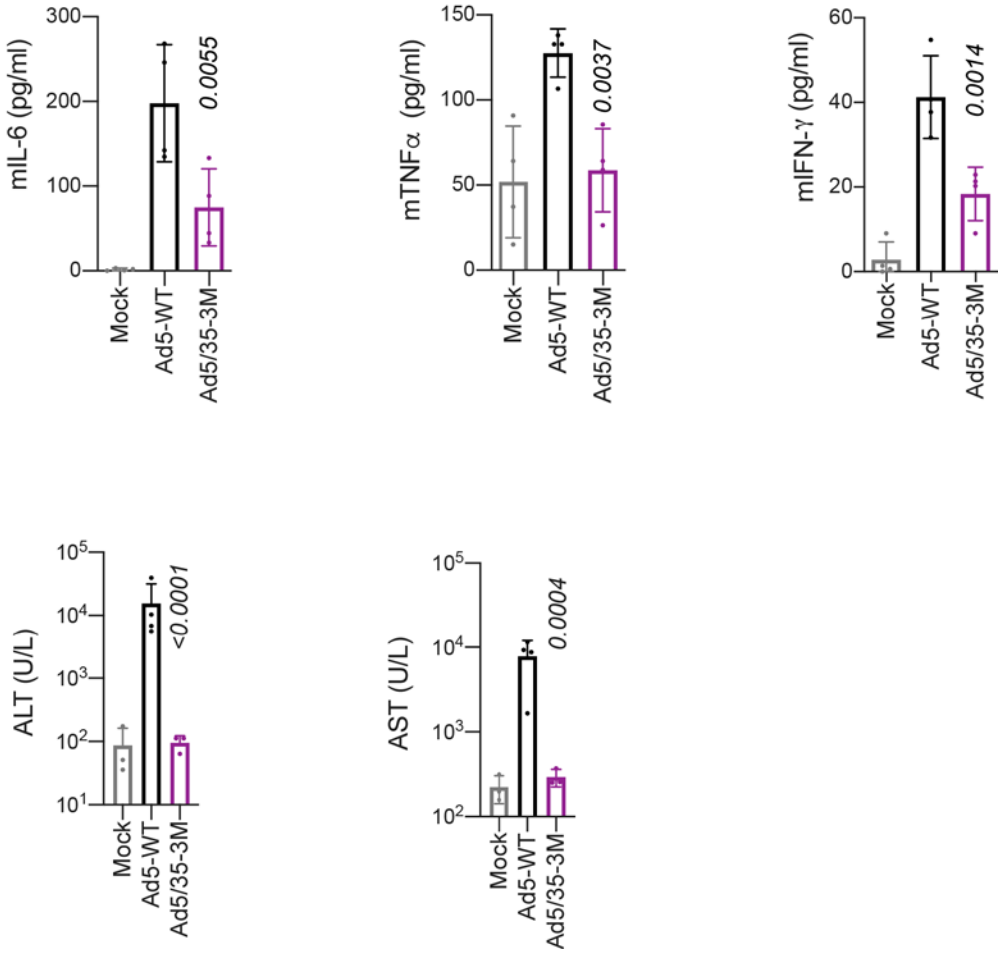

Fig. S14. Intravenous administration replication competent Ad5/35-3M virus does not trigger systemic toxicity. C57Bl6 mice were injected intravenously with $1x10^{11}$ vp of Ad5-WT, Ad5/35-3M, or virus-diluent buffer (Mock). Cytokines were measured in mouse plasma at 6 h post virus injection and the ALT/AST were measured at 48h post virus injection (n = 3-4). The p-values were calculated by one-way ANOVA test with multiple comparisons adjustments between Ad5-WT and Ad5/35-3M. Statistical details are in **Table S1**.

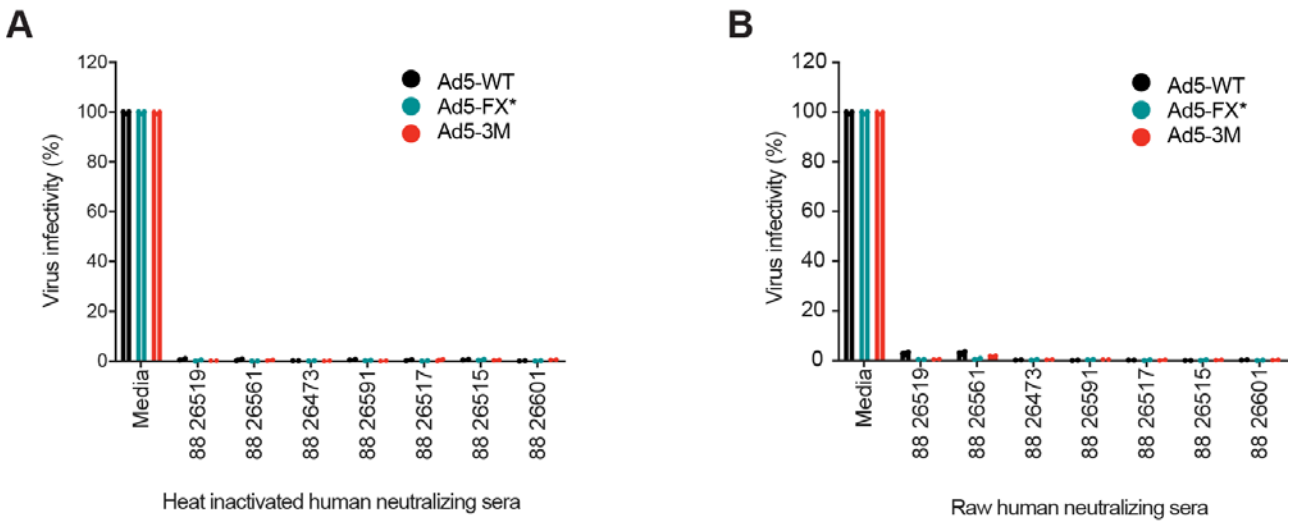

Fig. S15. Human sera with high HAdv-C5-specific neutralizing antibody titers neutralize Ad5-WT and capsid-modified adenoviruses. Indicated viruses were incubated with 90% of heat-inactivated (**A**) or raw (**B**) human sera from healthy volunteers containing high HAdv-C5-specific neutralizing activity (neutralizing Ab titers > 1:1000) and virus infectivity on HEK293 cells was compared to virus incubated in media with no serum addition.

Supplementary Tables

Mouse strain	Genotype	Also known as	Stock number
Rag-/-	B6.129S7-*Rag1tm1Mom*/J	Rag1 KO	002216
muMt-	B10.129S2(B6)-*Ighmtm1Cgn*/J	muMt-	002249
C3-/-	B6.129S4-*C3tm1Crr*/J	C3 KO	029661
CD36-/-	B6.129S1-*Cd36tm1Mfe*/J	CD36 KO	019006
CD18-/-	B6.129S7-*Itgb2tm2Bay*/J	CD18 KO	003329
ITGAM -/-	B6.129S4-*Itgamtm1Myd*/J	ITGAM	003991
NOD *scid* gamma	NOD.*Cg-PrkdcscidIl2rgtm1Wjl*/SzJ	NSG	005557
NCr nude, SPONTANEOUS MUTANT	CrTac:NCr-*Foxn1nu*	NCr Nude	NCRNU-F

Table S2. Mouse strains used in the study.

Antibody	Conjugate	Type	Clone	Company	Catalog number	Usage	Dilution
Anti-mouse F4/80	AF647	Rat IgG2a	BM8	Biolegend	123121	IF	1:100
Anti-mouse CD68	AF647	Rat IgG2a	FA-11	Biolegend	137003	IF	1:100
Anti-Mouse-C3	Biotin	Rat Mab	RmC11H9	Accurate Chemical and Scientific /Cedarlane	ACL7503B	ELISA	1:2000
Anti-Human/Mouse C3/C3b/iC3b	Biotin	Mouse IgG1	6C9	Cedarlane	CL7631B	ELISA	1:2000
Anti-Mouse-C4	Biotin	Rat Mab	RmC16D2	Accurate Chemical and Scientific /Cedarlane	ACL7504B	ELISA	1:2000
Anti-Mouse-CD36	None	Rat IgG2a	MF3	Bio-Rad	MCA2748GA	*In vivo* block	50 μg/mouse
Isotype Ctrl	None	Rat IgG2a	RTK2758	Biolegend	400516	*In vivo* block, control Ab	50 μg/mouse
Anti-Rabbit IgG (H+L)	AF594	Goat	Polyclonal	Jackson ImmunoResearch	111-585-003	IF, secondary	
Anti-Human Mitochondria	Cy3	Mouse	Clone 113-1	Millipore/Sigma	MAB1273C3	IF	1:100
Anti-Mouse IgM heavy chain	HRP	Goat	Polyclonal	Invitrogen	626820	ELISA	
Anti-Adenovirus Type 5	None	Rabbit	Polyclonal	Abcam	ab6982	IF	1:100

Table S3. List of antibodies used in the study

qPCR primers	Primer sequence
148.Human.dir	GCTGCTTCTCATTGTCTCGG
149.Mouse.dir	CCTGCTGCTTATCGTGGCTG
150.Human-mouse.rev	GCCAGGAGAATGAGGTGGTC
167.Human-mouse.dir	TACCTGCAGCTGTACGCCAC
15.Ad5_Qpcr-pol.dir	AAACGCCTTCCTGAGTACAC
16.Ad5_Qpcr-pol.rev	GTCTCAGTCACCATTAGCCG
190.Ad11-qpcr1.dir	AAAGCGTCTAACCAGTCACAG
191.Ad11-qpcr1.rev	ACCCAGACCGAACACATAAC
196.Ad35-qpcr1.dir	CATTCTCCTAAAGTCCAGCCC
197.Ad35-qpcr1.rev	TGAACATCCATACGGTCGAAC

Table S4. Sequences of the qPCR primers.